DOI: 10.1002/ejic.201000725

Flowerlike PbS Microcrystals: Citric Acid Assisted Synthesis, Shape Evolution, and Electrical Conductivities

Rencheng Jin,[a] Gang Chen,*[a] Qun Wang,[a] Jian Pei,[a] Gang Wang,[a] and Lin Wang[a]

Keywords: Lead sulfide / Hydrothermal synthesis / Facet-selective growth / Dissolution–recrystallization / Electrical conductivity

Lead sulfide (PbS) with various morphologies including flowerlike, microsphere, multipod, six-armed star, and truncated octahedron has been synthesized selectively under hydrothermal conditions. The synthesis procedure variables such as concentration of the citric acid (CA), kinds of surfactant, reaction temperature, and reaction time were observed to influence the resultant shape of PbS microstructures. The structure and morphology of the obtained products were characterized by means of X-ray diffraction (XRD), field-emission scanning electron microscopy (FESEM), transmission electron microscopy (TEM), energy-dispersive X-ray spectroscopy (EDS), and Fourier transform infrared spectroscopy (FTIR) analysis. On the basis of the time-dependent experimental data, the possible formation mechanism related to facet-selective growth and dissolution–recrystallization was presented. Furthermore, the electrical conductivities for different morphologies of PbS were measured to investigate the possible effect of morphology on the electrical conductivity.

Introduction

Recently, materials with different sizes and morphologies have attracted more and more interest due to their novel physical and chemical properties.[1–3] During the past few years, many efforts have been devoted to the design and synthesis of microcrystals and nanocrystals with various shapes such as nanorods, nanowires, nanocubes, nanobelts, nanotubes, hierarchical nanostructures, and star-shaped nanocrystals.[4] Even now, the synthesis of multimorphology particles with controllable shape is still an important and interesting topic. Binary lead chalcogenides are particularly important because they can be used in many aspects including thermoelectric (TE) and infrared (IR) photoelectric devices.[5] Thermoelectric devices are expected to play an increasingly important role in solving the energy crisis in the future. But their efficiency is low and cannot compete with conventional refrigerators and power generators at present. To enhance the thermoelectric figure of merit (ZT value) to achieve high-efficiency solid-state thermoelectric energy conversion, a decrease in the dimension of the materials is a good method that has been suggested by theoretical predications and experimental results.[6,7] Recent reports show that materials with different sizes and morphologies have a significant effect on the ZT value.[8–10] Therefore, it is essential to develop an alternative approach to prepare different sizes and shapes of thermoelectric materials to meet the demand of high-performance thermoelectric applications.

Lead sulfide, an important IV/VI semiconductor, has attracted considerable attention for its especially small direct bandgap (0.41 eV) and a large exciton Bohr radius (18 nm),[11] which has the potential to be used in thermoelectric devices,[12] infrared detectors,[13] sensors,[14] photographic equipment,[15] and solar cells.[16] Therefore, in recent years, the synthesis of PbS nano- and microcrystals has attracted intensive attention. For example, cube-shaped PbS micro- and nanocrystals have been synthesized by a solution-reflux method and the decomposition of a single-source precursor.[17,18] Rodlike PbS nanocrystals have been prepared by using cation-exchange reactions and a combination of surfactant and polymer matrix as a template.[19,20] Star-shaped PbS microcrystals have been obtained by a solution route.[17,21,22] Pyramidal PbS nanocrystals have been formed at the interface of toluene and water solutions.[23] PbS cubes with a hierarchical pyramidal pit on each face have been presented by a facile template-free solvothermal approach.[24] However, to date, there have been only limited reports on the synthesis of PbS three-dimensional (3D) superstructures composed of self-assembled low-dimensional (0D, 1D, 2D) nanostructures. In addition, few reports have been focused on the morphology-dependent electrical conductivity.

In this work, hierarchical flowerlike PbS microcrystals that consist of some self-assembled cubic crystals as well as microspheres, multipods, six-armed stars, and truncated octahedra have been synthesized by a quick, environmentally benign hydrothermal method. Some factors that affect

[a] Department of Chemistry, Harbin Institute of Technology, Harbin 150001, P. R. China
Fax: +86-451-86413753
E-mail: gchen@hit.edu.cn

Supporting information for this article is available on the WWW under http://dx.doi.org/10.1002/ejic.201000725.

the morphology of PbS crystals such as reaction temperature, the concentration of citric acid, kinds of surfactant, and reaction time are systematically investigated. A formation mechanism different from the traditional growth mechanism of *fcc* crystals is proposed. The mechanism related to facet-selective growth and dissolution–recrystallization is responsible for the surface energy controlled by the selective absorption of citrate. Moreover, the electric properties are investigated over the temperature range of 300–700 K to determine the impact of particle size and morphology on the electrical conductivity.

Results and Discussion

Structure and Morphology Analysis

The XRD pattern of the product is shown in Figure 1. All peaks can be indexed as face-centered cubic PbS with space group *Fm*3*m* (JCPDS, 05-0592). No peaks of impurities are detected, thereby indicating the high purity of the as-synthesized products. The apparent peaks are very strong and sharp, which suggests that the crystalline structures of the samples are perfect.

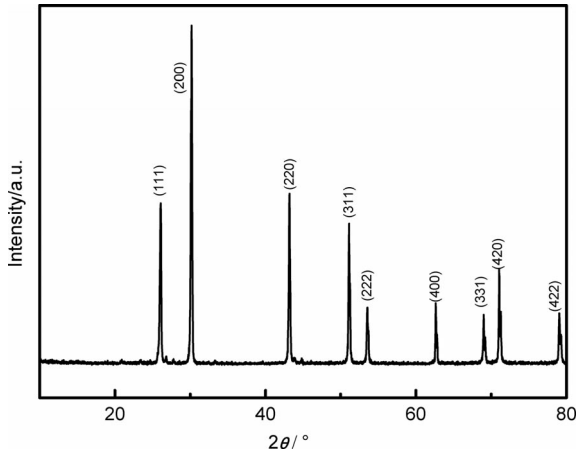

Figure 1. XRD pattern of PbS powder synthesized by a hydrothermal method at 180 °C for 1 h in the presence of citric acid.

The morphology and structure of brown PbS products have been measured by field-emission scanning electron microscopy (FESEM), TEM, and high-resolution transmission electron microscopy (HRTEM), Figure 2 demonstrates the microstructures of PbS synthesized at 180 °C for 1 h in the presence of citric acid. The low-magnification image in Figure 2a shows that the majority of the samples are composed of flowerlike crystals, which are uniform in size. The size distribution of the PbS microflowers has been evaluated from an analysis of FESEM images of at least 450 particles, and the results present that the size of the products is in the range of 0.7–3 μm (Figure 2b). Figure 2c is the high-magnification FESEM image of a flowerlike PbS microcrystal. Typically, this structure is composed of numerous intergrowth PbS subunits (cubic crystals) with a size of around 800 nm. The chemical composition of these PbS microflowers has been determined by energy-dispersive X-ray spectroscopy (EDS). The EDS spectrum (Figure 2d) demonstrates that the products are made of Pb and S only, and the atomic ratio of Pb/S is 51:49.

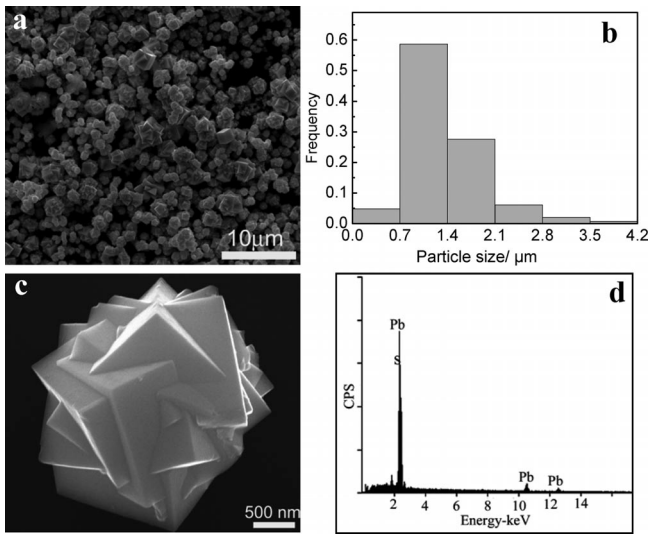

Figure 2. (a) Low-magnification FESEM image of flowerlike PbS microcrystals. (b) Size distribution of flowerlike PbS microcrystals. (c) High-magnification FESEM image of PbS microcrystals. (d) EDS spectrum of flowerlike PbS microcrystals prepared at 180 °C for 1 h in the presence of citric acid.

TEM and HRTEM analysis provide more detailed structural information of the particles. Figure 3a exhibits the TEM image of a single PbS microstructure, which is in accordance with the FESEM observations. This image demonstrates that the flower-shaped structures are made by some uniform cubic crystals, but the petals are not uniform in size. The high-crystalline nature of the petals has been determined by the HRTEM image (Figure 3b). The spacing between two neighboring fringes is 0.354 nm, which corresponds to the lattice spacing of the (111) planes in the face-centered cubic PbS. Its corresponding fast Fourier transform (FFT) pattern can be indexed to single crystalline, as presented in the inset of Figure 3b. All of these results show that the petal grows along the {111} plane.

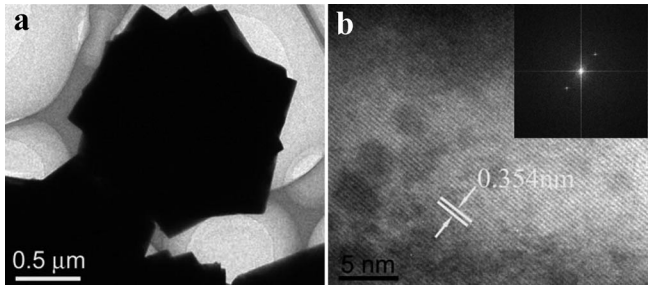

Figure 3. (a) TEM image of flowerlike PbS microstructures. (b) HRTEM image and its FFT pattern (inset) taken from the edge of a single petal of flowerlike PbS.

Investigation of Influencing Factors

A hydrothermal (or solvothermal) reaction is a complicated process, and a variety of factors can have an impact

Table 1. Synthesis conditions and characteristics of the samples prepared by means of the hydrothermal method.

Sample no.	Surfactant	Amount [g]	T [°C]/t [h]	Morphology	Reference
1	citric acid	0.4	140/1	multipod and flowerlike	Figure 4a
2	citric acid	0.4	180/1	flowerlike	Figure 2a
3	citric acid	0.4	240/1	flowerlike	Figure 4b
4	citric acid	0.1	180/1	microsphere	Figure 5a
5	citric acid	0.2	180/1	microsphere and flowerlike	Figure 5b
6	citric acid	0.6	180/1	hollow sphere	Figure 5c
7	no surfactant	0	180/1	eight-pod cubes	Figure 6a
8	CTAB[a]	0.2	180/1	truncated octahedron	Figure 6b
9	PVP[b]	0.2	180/1	cubic and irregular particles	Figure 6c
10	L-cysteine	0.2	180/1	six-armed starlike	Figure 6d
11	citric acid	0.4	180/0.5	quasi-sphere	Figure 8a
12	citric acid	0.4	180/2	flowerlike	Figure 8b
13	citric acid	0.4	180/4	flowerlike and microsphere	Figure 8c
14	citric acid	0.4	180/8	microsphere	Figure 8d

[a] CTAB = cetyltrimethylammonium bromide. [b] PVP = polyvinylpyrrolidone.

on the final morphology and structure of the products.[25] The morphology of the PbS microcrystals depends on many reaction factors, including synthesis temperature, the concentration of citric acid, and the kind of surfactant. All the factors are found to be interdependent, thus resulting in PbS microcrystals with different morphologies. The detailed morphology evolution for the samples is shown in Table 1. Among these factors, temperature is one of the most important ones during the synthesis procedure. Thus, the reactions have been carried out at 140, 180, and 240 °C, respectively, whereas other conditions are unchanged. By comparing the FESEM in Figure 4 and Figure 2a, one can see that the samples prepared at 180 °C are composed of the flowerlike crystals (Figure 2a). When the reaction was performed at a lower temperature (140 °C), multipod particles with hierarchical structures and some flower structures similar to the samples synthesized at 180 °C were obtained (Figure 4a). After increasing the temperature to 240 °C, only the irregular flowerlike structures were fabricated, as shown in Figure 4b. We speculate that the intensity of the coordination bond between Pb^{2+} and citric acid may be weakened at elevated temperatures, whereas the decomposition rate of thioacetamide is accelerated, which results in a relatively faster nucleation rate and growth rate of the particles. Meanwhile, the raw materials are consumed quickly with increasing temperature. As a result, PbS crystals with different morphologies and smaller size are obtained. A similar mechanism has been involved in the fabrication of Cu_2S and ZnO.[26,27]

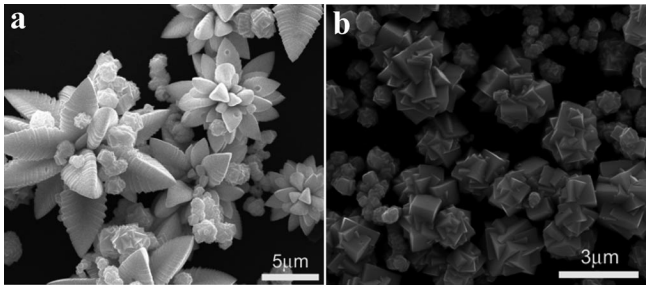

Figure 4. FESEM images of PbS crystals synthesized in the presence of citric acid at (a) 140 °C and (b) 240 °C for 1 h.

Citric acid, as a facet-selective absorption additive and chelating agent in the present experiment, can subtly affect the final morphologies of PbS microcrystals. Firstly, citric acid can coordinate with lead cations; the controlled release of lead cations from the lead citrate complex could decrease the formation rate of PbS crystallites. Secondly, according to the chelating properties of citrate, an increase in the citrate amount will decrease the interfacial free energies of the system.[28] In this work, we speculate that, during the growth of PbS nanocrystals, the citrate anions can selectively adsorb onto the different facets and change the growth rate in different directions. The two aspects are dynamically helpful to the effective subtle control of the morphologies of PbS microcrystals. We found that different shapes of PbS microcrystals were obtained with various concentrations of citric acid, as can be seen in Figure 5. Evidently, the concentration of the citric acid plays an important role in determining the morphology of the PbS microcrystals due to their preferentially selective adsorption on the {100} and {111} surface, which results in the different growth rate along the <100> directions to the <111> directions.[29] At the initial stage, a large amount of PbS nuclei grows into small seed particles, and as the reaction time is prolonged, the quasi-sphere seed particles aggregate thereby decreasing the surface energy.[30] When 0.1 g of citric acid is added, almost all of the citric acid coordinates with the lead cations, and no excess amount of citric acid adsorbs onto the PbS surface. It is reasonable to conclude that, in the current process, the seed particles prefer to aggregate together to reduce the surface energy, and microspheres of PbS are obtained. The SEM image of a sample is presented in Figure 5a. From the image one can see that the spherical particles with a rough surface are well separated from one another. From the image it can also be seen that the spherical particles are composed of many small PbS subunits (nanocrystals) with a size of around 15 nm (inset in Figure 5a). When the amount of the citric acid reaches 0.2 g, the remnant of that preferentially adsorbs onto some of the {100} faces of the subunits that

confine the crystal growth along the <100> directions; thus, microflowers composed of nanocubes and microsphere structures of PbS coexist (Figure 5b). When one continues to increase the amount of citric acid to 0.4 g, more citric acid in the solution absorbs onto the {100} face, which results in a higher growth rate along the <111> directions; then microcrystals composed of flowerlike PbS appear (Figure 2a). By further increasing the citric acid amount to 0.6 g, enough citric acid molecules that exist in the solution can bind to each crystal surface of the PbS nuclei, which leads to an isotropical growth of PbS. Simultaneously, small nanoparticles of PbS could assemble together due to the hydrogen-bond and electrostatic effects of citric acid anions. However, due to the steric effect of citric acid molecules, the assembled nanoparticles are loosely compacted, and many voids exist. In addition, the aggregated PbS nanoparticles are not stable because of their high surface energy.[31] Thus, the larger particles become thermodynamically preferred, and then the conversion from loosely packed spherical particles to hollow structures through Ostwald ripening can be seen, as illustrated in the SEM image of Figure 5c. Similar mechanisms have been reported in the synthesis of Fe_3O_4, Cu_2O, and $CdMoO_4$ hollow spheres.[32–34] Different morphologies of the samples with different concentrations of the surfactant were also reported by Liang and co-workers.[35] They demonstrated that oleic acid could selectively adsorb onto {100}, {111}, and {110} surfaces with increasing concentration, thereby resulting in different growth rates along different surfaces, and therefore microcubes, microoctahedra, truncated octahedra, and microrhombic dodecahedra of Cu_2O were formed. According to the above experimental results and analysis, the formation of different shapes of PbS is ascribed to the strong interaction between the surface of PbS particles and citric acid molecules. This observation suggests that the concentration of citric acid is indispensable to the formation of the PbS structures.

The kind of surfactant can also significantly affect the shape of the final products. To ascertain the effect of the surfactant on the morphology, a series of contrastive experiments were performed. When no surfactant was added, eight-pod cubes of PbS were gained, as can be seen in Figure 6a. In the absence of any surfactant, the preferential growth orientation along <111> rather than <100> first led to the formation of cubes. As crystal growth proceeded, the size of the PbS crystal became larger, and thus the mass transport became much more difficult, thereby resulting in the formation of eight-pod cubes of PbS because of the Berg effect,[36] that is, the growth rate of the edge of the {111} plane was faster than that of the {100} inner plane. In the presence of CTAB, uniformly truncated octahedral particles were obtained. Figure 6b presents a typical SEM image of well-defined truncated octahedra of PbS synthesized in the presence of CTAB. As shown in the low-magnification SEM image, the as-prepared products consisted of a large quantity of well-defined truncated octahedra of PbS with a size of 0.5–1 μm. During the process, CTAB was in fact used as a capping agent to stabilize the growth of PbS

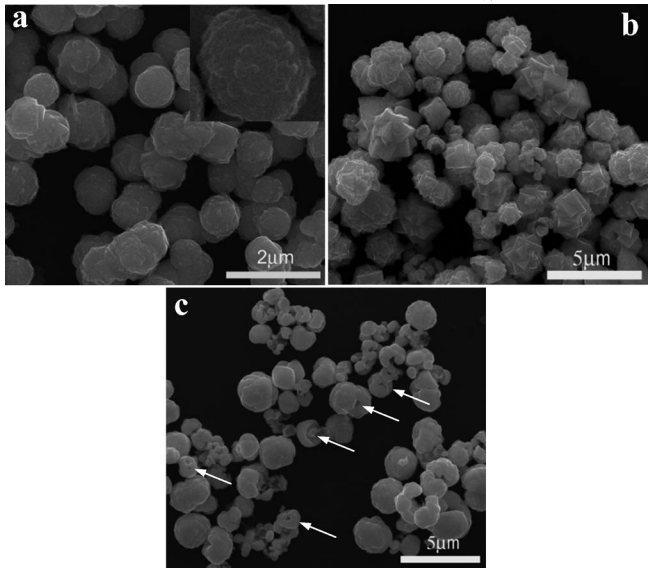

Figure 5. FESEM images of PbS crystals synthesized in different concentrations of citric acid: (a) 0.1 g, (b) 0.2 g, and (c) 0.6 g.

crystals;[37] a strong interaction exists between the nitrogen atoms of CTAB and the {100} and {111} facets, which indicates that the PbS grows simultaneously along the <100> and <111> directions. When polyvinylpyrrolidone (PVP) was added into the solution instead of CTAB, a different morphology of PbS formed. A typical image of the products is shown in Figure 6c. It shows cubic PbS and some irregular particles. As a polymer surfactant, PVP molecules with long chains can be adsorbed onto the PbS particle surfaces through physical and chemical bonding. It is believed that PVP tends to inhibit the growth rate of the {100} facets more than that of the {111} facets, since it is expected to absorb at the {100} facets of *fcc* geometry of PbS because of its carbonyl group.[38] And then cubes of PbS are obtained. On the other hand, as a weakly bound ligand to the PbS crystal, desorption of PVP from the PbS surface will form, and the nanocubes will assemble together to decrease the surface energy, thereby resulting in some aggregated cubic shapes of PbS. Figure 6d is the SEM image of PbS crystals when using L-cysteine as the surfactant; the as-prepared products are composed of a large quantity of six-armed starlike PbS nanostructures around 1.5 μm in length and 600 nm in width. In fact, as a surfactant, L-cysteine can adsorb onto both the {100} and {111} facets, because different functional groups such as the nitrogen atoms and carbonyl groups coexist in the L-cysteine molecule, which may lead first to the formation of octahedra (or truncated octahedra) of PbS. In addition, L-cysteine can be used as a sulfur resource; the decomposition of L-cysteine and thioacetamide accelerate the nucleation and growth rate, and octahedral (truncated octahedral) PbS continues to be inclined to grow along the <100> orientation, specifically along the six apical directions of the octahedron (truncated octahedron), which leads to a large size distribution of PbS crystals and the interesting six-armed starlike structure.

Similar star-shaped structures formed by the growth of six horns out along the [100] direction were reported by Warner et al. and Cheon et al.[39,40]

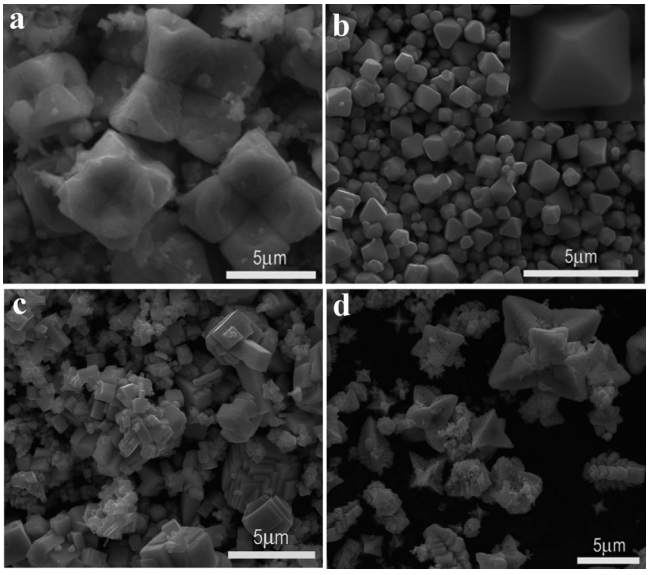

Figure 6. FESEM images of PbS products in the presence of (a) no surfactant, (b) CTAB, (c) PVP, and (d) L-cysteine at 180 °C for 1 h.

To demonstrate the surface adsorption of the surfactant on PbS microcrystals, FTIR spectral studies of PbS microcrystals, prepared in the presence of various surfactants, were performed. Figure 7a shows the FTIR spectrum of PbS with the assistance of PVP. From the image it can be clearly seen that there is no obvious peak in the spectrum, which indicates that the PVP molecules can be easily washed away from the surface of PbS. And it further proves that a desorption of PVP from the surface of PbS occurred, which is in accordance with what has been discussed above. When CTAB was used as surfactant, the obvious peaks in Figure 7b at 1060 and 1172 cm^{-1} match with the C–N^+ stretching vibration, which clearly demonstrates that the head groups of CTAB molecules are directed toward the PbS surface. Similar results have been reported in the synthesis of PbS microcrystals by using DTAB as a surfactant by Petersen's research group.[41] The weak peak in Figure 7b at 2931 cm^{-1} can be attributed to the C–H stretching vibration. When L-cysteine is used as the surfactant, only one weak peak at 2914 cm^{-1} that belongs to the C–H stretching vibration can be seen (Figure 7c). Figure 8d is the FTIR spectrum of PbS, which was prepared by using citric acid as surfactant instead of others. The interaction between citric acid and PbS microcrystals has also been verified by the C–H stretching vibration at 2907 cm^{-1} and the characteristic peaks of the carboxy group (–COOH) around 3420 cm^{-1} (Figure 8d) in the FTIR spectrum.

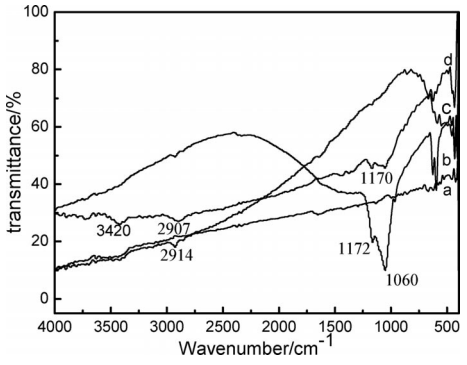

Figure 7. FTIR spectra of PbS crystals synthesized with various surfactants (a) PVP, (b) CTAB, (c) L-cysteine, and (d) citric acid.

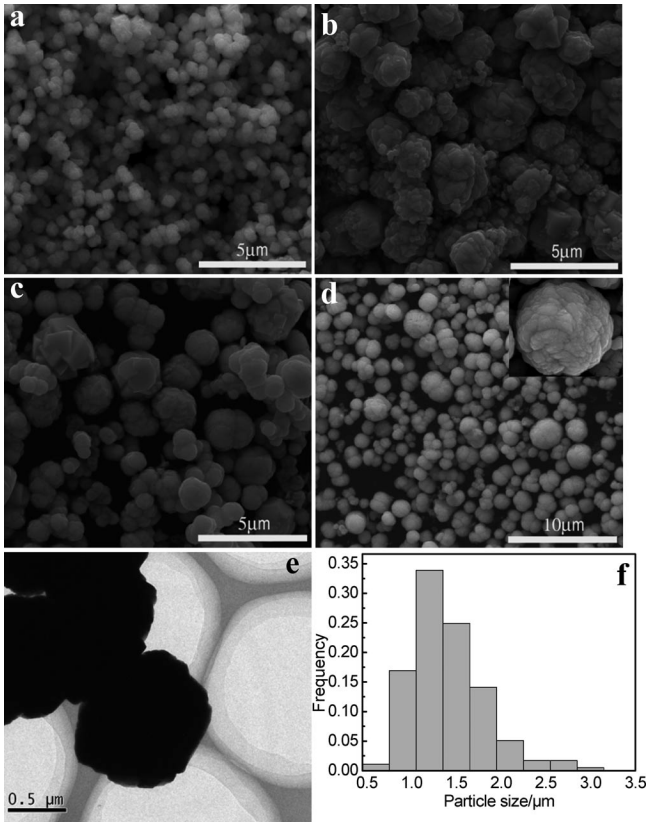

Figure 8. FESEM images of samples prepared at different reaction times: (a) 0.5 h, (b) 2 h, (c) 4 h, and (d) 8 h.

Growth Mechanism of PbS Crystals

To further understand the formation mechanism of the PbS crystals, time-dependent experiments were carried out at 180 °C for 0.5, 1, 2, 4, and 8 h in the presence of citric acid. Figure 8 displays the FESEM images of PbS obtained at different reaction times. When the reaction time was 0.5 h, aggregated quasi-sphere structures of PbS with an average diameter of about 300–500 nm could be found (Figure 8a). The surface of the particles is rough, which indicates that the quasi-spherical aggregates should be composed of many small nanoparticles. As the reaction time was increased, the quasi-spherical aggregates changed; Figure 2a shows that the samples prepared for 1 h are composed of a flowerlike structure, and the size is in the range between 0.7 and 3 μm. The structure is composed of densely

packed nanocubes. By increasing the reaction time to 2 h, the petals (Figure 8b) became smaller, and more petals formed relative to Figure 2a. At the same time, the smooth surface became rough again. By further increasing the reaction time to 4 h, the petals of the flower almost disappeared, microspheres of PbS were obtained, and a few flowerlike structures were occasionally found, which can be seen clearly in Figure 8c. When the reaction time reached 8 h, well-defined microspheres formed (Figure 8d). The image inset in Figure 8d shows that the surface of the PbS microspheres is rough, which implies that the outside of the sphere is composed of many nanoparticles. Figure 8e and f represent the TEM image and size distribution of the as-prepared samples. It can be seen here that the microsphere structure of PbS is in agreement with the FESEM observations with an average size of 1.5 μm. As a result, the formation equation of the reaction system may be formulated as follows [Equation (1)].

$$Pb^{II} + CA \rightarrow Pb^{II}(CA)$$
$$CH_3CSNH_2 + H_2O \rightarrow CH_3CONH_2 + 2\,H^+ + S^{2-}$$
$$Pb^{II}(CA) + S^{2-} \rightarrow PbS + CA \quad (1)$$

Generally, the growth process of lead chalcogenide crystals includes two stages:[42,43] the initial nucleating stage and a subsequent growth stage. During nucleation, the seeds crystallize as polyhedrons, which exposes six {100} and eight {111} facets because of their highly symmetric cubic rocksalt crystal structures. At the growth stage, growth rates on different facets are determined by the surface energy. As a facet-centered cubic structure, the energy of the {111} facets is higher than that of the {100} ones, thus resulting in a faster growth rate along the [111] direction than in the [100] direction. In a solution-phase synthetic process, impurities and surfactants are often used to alter the surface energies through adsorption or chemical interaction, and thus new shapes of the particles come into being. But on the basis of the above investigation, the mechanism of the growth stage is different. In our case, citric acid is used as chelating agent and surfactant. In aqueous solution, carboxy groups can form complexes with lead cations through coordination interaction, which greatly decreases the free Pb^{2+} ion concentration in solution. Such a low concentration of lead cations leads to a relatively slow nucleation rate and facilitates the growth of PbS nanocrystals in view of the dynamic process. During the growth stage, the reduction in surface energy is believed to be the primary driving force for simple particle growth; thus, the nuclei assemble together to form quasi-sphere nanoparticles; because of the hydrogen-bond and electrostatic effects of the citric acid anions,[44] the quasi-sphere nanoparticles agglomerate. As the reaction time is prolonged, the molar ratio of citric acid to lead cations increases, which leads to a low free Pb^{2+} ion concentration in solution, thereby further slowing the reaction rate and facilitating the preferential growth of PbS. Furthermore, the carboxy groups can adsorb onto the {100} facets more strongly than onto others, and thus efficiently inhibit the growth rate along {100} facets, which leads to a faster growth rate along the <111> directions than along the <100> directions. Thus, flowerlike PbS is obtained. A similar phenomenon was also observed in the studies of star-shaped and rod-based multipod PbS nanocrystals and Bi_2S_3 nanoflowers.[45,46] As the aging time increased, part of the corners and edges of the flowerlike microcrystals dissolved into smaller nanocrystals and minimized the surface energy. Crystal growth then followed, and larger particles grew at the expense of smaller nanocrystals with the assistance of citrate. The surface of the particles became rough, and a surface recrystallization process took place, thus leading to the formation of PbS microspheres. From our experimental results and the above discussion we consider that the time-dependent morphology-evolution process of PbS can be illustrated in Figure 9.

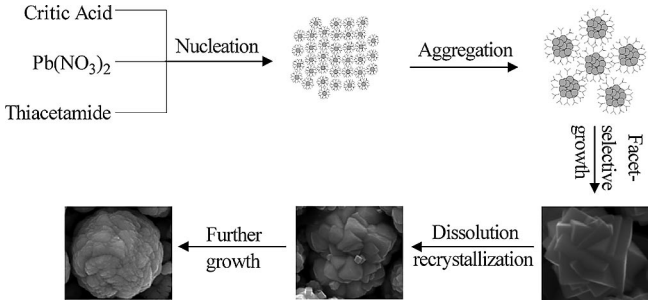

Figure 9. Morphology-evolution process of PbS crystals.

In summary, there are two key factors that determine the final morphologies of PbS microcrystals. The first is the citrate anions used as chelating agents and morphology modifiers, which play a key role in controlling the nucleation rate and suppressing the growth rate along different directions. The second one is the dissolution–recrystallization process, which is responsible for the transformation from microflower to microsphere.

Electrical Conductivity of PbS Crystals

Recently reported efforts to prepare thermoelectic (TE) materials from chemically synthesized nanocrystals (NCs) revealed serious challenges that were mainly associated with the presence of organic molecules (surface ligands or molecular capping agents) at the NC surface.[47–49] Being vitally important for NC synthesis, these organic molecules are highly insulating and hamper the electrical conductivity of NC solids.[47] Talapin et al. and Wang et al. also reported that removing the fraction of the capping groups would reduce the interparticle spacing and yield a higher conductivity.[48,49] Therefore, in our studies, the annealing experiments at 250 °C for 4 h under argon to remove the organic molecules from the surface of PbS microcrystals were carried out before electrical conductivity measurements. The complete removal of the surface ligand was confirmed by comparing the FTIR spectra for their flowerlike PbS NC solids before and after the thermal treatments in Figure 10. The obvious difference in the spectra is the absence of the C–H stretching vibration at 2907 cm^{-1} and the characteristic peaks of the carboxy group (–COOH) around

3420 cm^{-1}, which illustrates the pyrolysis of citric acid. The other peak at about 1170 cm^{-1} in the spectra corresponds to PbS.[50,51] Moreover, the microspheres of PbS annealed under the same conditions. Additionally, the microflowers and microspheres of PbS were pressed into a strip with a rectangular shape of about $10 \times 4.6 \times 1.2$ mm for the measurement of electrical conductivity. Figure 11 shows the temperature-dependent electrical conductivity of the microflowers and microspheres of PbS crystals. It can be clearly seen that the electrical conductivity of the two samples monotonically increases with increasing temperature, which indicates the typical electrical conductivity of a semiconductor. As is shown in the image, the electrical conductivity of flowerlike PbS was 5.5 $S cm^{-1}$ at 690 K, whereas the electrical conductivity of PbS microspheres was only 1.29 $S cm^{-1}$ at the same temperature. Recently, Toprak et al. proposed that the size and grain boundaries have a sizeable effect on the electrical conductivity.[52] The electrical conductivity is low for products with smaller particle size.

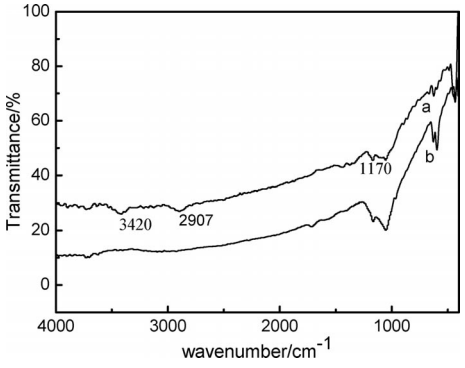

Figure 10. (a) FTIR spectra of flowerlike PbS microcrystals and (b) FTIR spectra of flowerlike PbS microcrystals after annealing at 250 °C under argon.

In our experiments, the surface of the PbS microspheres was composed of many nanoparticles, which may have resulted in more grain boundaries in the pressed strip. And this may have led to the reduction of the carrier mobility due to the scattering of the charge carrier by enhancing the density of grain boundaries for smaller grains, which is in accordance with the results reported by Liu et al. and Luther et al.[53,54] To validate this argument, SEM images of the fractured surface of PbS after annealing were measured; they are shown in Figure 12. As indicated in the figure, the grain size of the flowerlike PbS is above 5 μm (Figure 12a), which is much larger then that of the microsphere PbS (Figure 12b). For the two different morphologies of PbS, samples with a larger grain size show higher electrical conductivity over the measured temperature range. A similar influence of grain size and grain boundaries on the electrical conductivity has also been reported by Zhao et al.[55] and our research group.[56] Additionally, to determine whether or not there is phase transformation during annealing, we measured the XRD of PbS microspheres and flowerlike crystals collected after the measurement of electrical conductivity at a temperature of 700 K for about 3 h under argon (Figure 11b). The results demonstrate that the above samples after annealing are consistent with the PbS structure, which indicates that these samples have a good thermal stability. To further understand the effects of morphology on electrical conductivity, different shapes of PbS such as nanocubes, six-armed stars, truncated octahedra, and so on were also measured under the same conditions. As shown in Figure S1 in the Supporting Information, the temperature dependence of the electrical conductivities of the above five samples is similar to those of PbS microspheres and flowerlike crystals. According to the results depicted in Figure S1, the electrical conductivity of the sample is proportional to the diameter (size). The diameter of eight-pod cubes is obviously larger than that of six-armed stars, truncated octahedra, and nanocubes. That is why it possesses a higher electrical conductivity. From another point of view, electrical conductivity is also dependent on the density of the specimen; the higher the density a specimen has, the (slightly) higher electrical conductivity it will have relative to that of the lower-density specimen.[57] In our case, the petals of flowerlike PbS may have been more fragile during pressing, and less void space existed in the

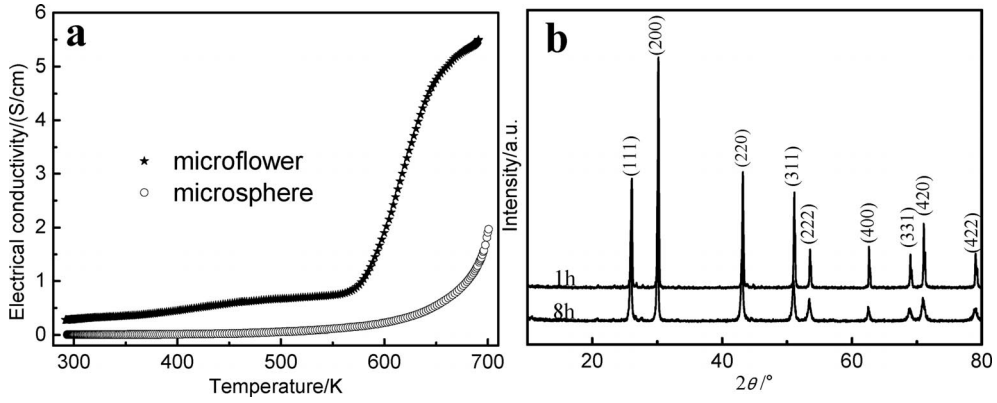

Figure 11. (a) Temperature dependence of the electrical conductivities for flowerlike and microsphere PbS crystals. (b) XRD pattern of microflower and microsphere PbS collected after the measurement of electrical conductivity at a temperature of 700 K under argon for 3 h.

strip, which led to the higher electrical conductivity of flowerlike PbS than that of the PbS eight-pod cubes and six-armed star morphologies. According to the above discussion, the smaller size and the lower density of the sample will obviously reduce the conductivity; thus, one can consider that the electrical conductivity of the hollow structure composed of nanoparticles is much lower than that of other shapes. As shown in Figure S1, the experimental conductivity of the hollow sphere is in accordance with the prediction and presents only 1.0 $S cm^{-1}$ at 690 K. Moreover, the measured electrical conductivities of all the samples at room temperature are more than 10 times lower than those of the PbS single nanowire of Lau et al. and Fardy et al.,[58,59] and 100 orders of magnitude higher than those of quantum-confined PbS nanocrystals.[60] A possible explanation for the observed shape dependence of the electrical conductivity originates in the grain boundaries. The axial electrical conductivity of PbS nanowires measured in the literature is high, because no obvious grain boundaries are observed. With an increase in the grain boundaries, the electrical conductivities might decrease. According to the electrical conductivity obtained in our experiments and that, which exists in the literature, we posit that the bulk PbS may present a higher electrical conductivity if no defects exist.

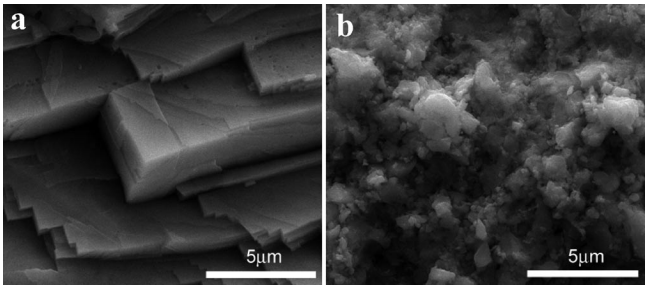

Figure 12. FESEM images of a typical fractured surface of PbS after annealing: (a) microflower and (b) microsphere.

Conclusion

In this paper, different morphologies of PbS nano- and microstructures have been synthesized by means of a quick, citric acid assisted hydrothermal method. Unlike other types of surfactant, it is found that the citric acid plays an important role in the synthesis of flowerlike PbS, in which it is used as chelating agent and capping agent. The shape evolution of PbS microcrystals can be controlled by the different growth ratio between the [111] and the [100] direction and the dissolution–recrystallization process. Evidently, the electrical conductivity of PbS microcrystals is dependent on the morphology. The flowerlike PbS offers a higher electrical conductivity than that of other morphologies, which may have potential use in the design of PbS crystals with desirable shapes for the fabrication of advanced thermoelectrical devices.

Experimental Section

Chemicals: All reagents were of analytical grade and used as received. Lead nitrate, thioacetamide, citric acid, cetyltrimethylammonium bromide (CTAB), polyvinylpyrrolidine (PVP, K-30, $M_r \approx 40000$), and L-cysteine were purchased from Shanghai Chemical Reagent Co. Water used in the experiment was obtained with a water-purification appliance.

Preparation of PbS Particles: In a typical procedure, lead nitrate (0.19 g) and citric acid (0.4 g) were dissolved in distilled water (10 mL). Under constant stirring, thioacetamide (0.075 g) was added. After stirring for 5 min, the solution was transferred into a 40 mL Teflon-lined stainless steel autoclave, and distilled water was added again up to 80% capacity of the total volume of the autoclave. The autoclave was sealed and heated at 180 °C for 1 h and then cooled to room temperature naturally. Brown precipitates were obtained by centrifugation, and then washed with ethanol and distilled water several times. After that, the products were dried in a vacuum at 60 °C for 6 h. To study the growth mechanism of the as-prepared products, the reaction time, temperature, concentration of citric acid, and the kinds of surfactant (CTAB, PVP, and L-cysteine) were systematically varied.

Characterization: The phase structures of the as-prepared samples were measured with a powder X-ray diffractometer (XRD, Rigaku D/max-2000) using monochromated Cu-K_α radiation. The X-ray tube was operated at 40 kV and 50 mA. The scan speed was 4° min^{-1}. Scanning electron microscopy measurements were carried out with an FEI Quanta 200F instrument using an accelerating voltage of 20 kV. Transmission electron microscopy and high-resolution transmission electron microscopy were performed with an FEI Tecnai G2 S-Twin instrument operating at 300 kV. Infrared absorption was performed with an FTIR spectrometer (Shimadzu) in the range of 400–4000 cm^{-1} in the form of KBr pellets.

Measurement of Electrical Conductivity: To measure the electrical conductivity of the PbS powders, a pressed strip of samples ($10 \times 4.6 \times 1.2$ mm) was prepared under pressure after annealing at 250 °C for 4 h with a flow of argon at 10 mL min^{-1}. A similar method can be found in our previous work.[56] The electrical conductivities were tested by a computer-assisted DC four-probe technique with a 2400 sourcemeter (Keithley 2700, Keithley Instruments Inc., America) under argon. The temperature was changed from 300 to 700 K at a rate of 1.5 K min^{-1}.

Supporting Information (see also the footnote on the first page of this article): Temperature dependence of the electrical conductivities for different morphologies of PbS crystals.

Acknowledgments

This work was supported by the National Natural Science Foundation of China (project no. 20871036), and the Development Program for Outstanding Young Teachers at the Harbin Institute of Technology (HITQNJS.2009.001).

[1] Y. N. Xia, P. D. Yang, Y. G. Sun, Y. Y. Wu, B. Mayers, B. Gates, Y. D. Yin, F. Kim, Y. Q. Yan, *Adv. Mater.* **2003**, *15*, 353–389.
[2] J. Zhang, L. Sun, J. Yin, H. Su, C. Liao, C. Yan, *Chem. Mater.* **2002**, *14*, 4172–4177.
[3] J. Geng, D. Lu, J. Zhu, H. Chen, *J. Phys. Chem. B* **2006**, *110*, 13777–13785.
[4] C. Burda, X. Chen, R. Narayanan, M. A. El-Sayed, *Chem. Rev.* **2005**, *105*, 1025–1102.

[5] T. C. Harman, P. J. Taylor, M. P. Walsh, B. E. LaForge, *Science* **2002**, *297*, 2229–2232.
[6] A. I. Hochbaum, R. K. Chen, R. D. Delgado, W. J. Liang, E. C. Garnett, M. Najarian, A. Majumdar, P. D. Yang, *Nature* **2008**, *451*, 163–167.
[7] Y. M. Lin, M. S. Dresselhaus, *Phys. Rev. B* **2003**, *68*, 075304.
[8] G. A. Tai, W. L. Guo, Z. H. Zhang, *Cryst. Growth Des.* **2008**, *8*, 2906–2911.
[9] S. Y. Jang, H. S. Kim, J. Park, M. Jung, J. Kim, S. H. Lee, J. Roh, W. Lee, *Nanotechnology* **2009**, *20*, 415204.
[10] J. P. Heremans, V. Jovovic, E. S. Toberer, A. Saramat, K. Kurosaki, A. Charoenphakdee, S. Yamanaka, G. J. Snyder, *Science* **2008**, *321*, 554–557.
[11] J. L. Machol, F. W. Wise, R. C. Patel, D. B. Tanner, *Phys. Rev. B* **1993**, *48*, 2819–2822.
[12] J. Androulakis, C. H. Lin, H. J. Kong, C. Uher, C. I. Wu, T. Hogan, B. A. Cook, T. Caillat, K. M. Paraskevopoulos, M. G. Kanatzidis, *J. Am. Chem. Soc.* **2007**, *129*, 9780–9788.
[13] P. Gadenne, Y. Yagil, G. J. Deutscher, *J. Appl. Phys.* **1989**, *66*, 3019–3025.
[14] F. Patolsky, G. Zheng, O. Hayden, M. Lakadamyali, X. Zhuang, C. Lieber, *Proc. Natl. Acad. Sci. USA* **2004**, *101*, 14017–14022.
[15] P. K. Nair, O. Gomezdaza, M. T. S. Nair, *Adv. Mater. Opt. Electron.* **1992**, *1*, 139–145.
[16] O. Hayden, R. Agarwal, C. M. Lieber, *Nat. Mater.* **2006**, *5*, 352–356.
[17] T. Trindade, P. O'Brien, X. M. Zhang, M. Motevalli, *J. Mater. Chem.* **1997**, *7*, 1011–1016.
[18] G. J. Zhou, M. K. Lu, Z. L. Xiu, S. F. Wang, H. P. Zhang, Y. Y. Zhou, S. M. Wang, *J. Phys. Chem. B* **2006**, *110*, 6543–6548.
[19] J. M. Luther, H. M. Zheng, B. Sadtler, A. P. Alivisatos, *J. Am. Chem. Soc.* **2009**, *131*, 16851–16857.
[20] S. Wang, S. Yang, *Langmuir* **2000**, *16*, 389–397.
[21] Y. Ma, L. Qi, J. Ma, H. Cheng, *Cryst. Growth Des.* **2004**, *4*, 351–354.
[22] Y. Ni, H. Liu, F. Wang, Y. Liang, J. Hong, X. Ma, Z. Xu, *Cryst. Growth Des.* **2004**, *4*, 759–764.
[23] D. B. Fan, P. J. Thomas, P. O'Brien, *J. Am. Chem. Soc.* **2008**, *130*, 10892–10894.
[24] Y. L. Hou, H. Kondoh, T. Ohta, *Cryst. Growth Des.* **2009**, *9*, 3119–3123.
[25] J. Xu, D. F. Xue, *J. Phys. Chem. B* **2006**, *110*, 7750–7756.
[26] Z. Fang, X. Y. Wang, J. M. Shen, X. Lin, Y. H. Ni, X. W. Wei, *Cryst. Growth Des.* **2010**, *10*, 469–474.
[27] X. Q. Meng, D. X. Zhao, J. Y. Zhang, D. Z. Shen, Y. M. Lu, Y. C. Liu, X. W. Fan, *Chem. Phys. Lett.* **2005**, *407*, 91–94.
[28] Z. R. Tian, J. A. Voigt, J. Liu, B. Mckenzie, M. J. Mcdermott, M. A. Rodriguez, H. Konishi, H. F. Xu, *Nat. Mater.* **2003**, *2*, 821–826.
[29] Z. L. Wang, *J. Phys. Chem. B* **2000**, *104*, 1153–1175.
[30] W. G. Lu, J. Y. Fang, *J. Phys. Chem. B* **2005**, *109*, 19219–19222.
[31] J. Yu, H. Guo, S. A. Davis, S. Mann, *Adv. Funct. Mater.* **2006**, *16*, 2035–2041.
[32] D. B. Yu, X. Q. Sun, J. W. Zou, Z. R. Wang, F. Wang, K. Tang, *J. Phys. Chem. B* **2006**, *110*, 21667–21671.
[33] H. T. Zhu, J. X. Wang, G. Y. Xu, *Cryst. Growth Des.* **2009**, *9*, 633–638.
[34] W. S. Wang, L. Zhen, C. Y. Xu, B. Y. Zhang, W. Z. Shao, *J. Phys. Chem. B* **2006**, *110*, 23154–23158.
[35] X. D. Liang, L. Gao, S. W. Yang, J. Sun, *Adv. Mater.* **2009**, *21*, 2068–2071.
[36] H. R. Liu, W. F. Miao, S. Yang, Z. M. Zhang, J. F. Chen, *Cryst. Growth Des.* **2009**, *9*, 1733–1740.
[37] L. Zhang, C. Z. Huang, Y. F. Li, Q. Li, *Cryst. Growth Des.* **2009**, *9*, 3211–3217.
[38] G. Zhang, X. Lu, W. Wang, X. Li, *Chem. Mater.* **2007**, *19*, 5207–5209.
[39] J. H. Warner, H. Q. Cao, *Nanotechnology* **2008**, *19*, 305605.
[40] S. M. Lee, Y. W. Jun, S. N. Cho, J. Cheon, *J. Am. Chem. Soc.* **2002**, *124*, 11244–11245.
[41] M. S. Bakshi, P. Thakur, S. Sachar, G. Kaur, T. S. Banipal, F. Possmayer, N. O. Petersen, *J. Phys. Chem. C* **2007**, *111*, 18087–18098.
[42] T. Mokari, M. J. Zhang, P. D. Yang, *J. Am. Chem. Soc.* **2007**, *129*, 9864–9865.
[43] T. J. Zhu, X. Chen, Y. Q. Cao, X. B. Zhao, *J. Phys. Chem. C* **2009**, *113*, 8085–8091.
[44] J. Pan, S. L. Xiong, B. J. Xi, J. F. Li, J. Y. Li, H. Y. Zhou, Y. T. Qian, *Eur. J. Inorg. Chem.* **2009**, *35*, 5302–5306.
[45] Y. W. Jun, J. S. Choi, J. W. Cheon, *Angew. Chem. Int. Ed.* **2006**, *45*, 3414–3439.
[46] J. Tang, A. P. Alivisatos, *Nano Lett.* **2006**, *6*, 2701–2706.
[47] A. Purkayastha, F. Lupo, S. Kim, T. B. Tasciuc, G. Ramanath, *Adv. Mater.* **2006**, *18*, 496–500.
[48] D. V. Talapin, C. B. Murray, *Science* **2005**, *310*, 86–88.
[49] R. Y. Wang, J. P. Feser, J. S. Lee, D. V. Talapin, R. Segalman, A. Majumdar, *Nano Lett.* **2008**, *8*, 2283–2288.
[50] N. N. Parvathy, G. M. Pajonk, A. V. Rao, *J. Cryst. Growth* **1997**, *179*, 249–257.
[51] H. Cao, G. Wang, S. Zhang, X. Zhang, *Nanotechnology* **2006**, *17*, 3280–3287.
[52] M. S. Toprak, C. Stiewe, D. Platzek, S. Williams, L. Bertini, E. Müller, C. Gatti, Y. Zhang, M. Rowe, M. Muhammed, *Adv. Funct. Mater.* **2004**, *14*, 1189–1196.
[53] Y. Liu, M. Gibbs, J. Puthussery, S. Gaik, R. Ihly, H. W. Hillhouse, M. Law, *Nano Lett.* **2010**, *10*, 1960–1969.
[54] J. M. Luther, J. B. Gao, M. T. Lloyd, O. E. Semonin, M. C. Beard, A. J. Nozik, *Adv. Mater.* **2010**, *22*, 3704–3707.
[55] L. D. Zhao, B. P. Zhang, W. S. Liu, J. F. Li, *J. Appl. Phys.* **2009**, *105*, 023704.
[56] L. Wang, G. Chen, Q. Wang, H. J. Zhang, R. C. Jin, D. H. Chen, X. B. Meng, *J. Phys. Chem. C* **2010**, *114*, 5827–5834.
[57] J. Martin, G. S. Nolas, W. Zhang, L. Chen, *Appl. Phys. Lett.* **2007**, *90*, 222112.
[58] Y. K. A. Lau, D. J. Chernak, M. J. Bierman, S. Jin, *J. Mater. Chem.* **2009**, *19*, 934–940.
[59] M. Fardy, A. I. Hochbaum, J. Goldberger, M. M. Zhang, P. D. Yang, *Adv. Mater.* **2007**, *19*, 3047–3051.
[60] M. H. Zarghami, Y. Liu, M. Gibbs, E. Gebremichael, C. Webster, M. Law, *ACS Nano* **2009**, *4*, 2475–2485.

Received: July 2, 2010
Published Online: November 12, 2010

